Synthesis, characterization, and photodegradation assessment of Ni and Cd-doped TiO$_2$ nanocrystals via sol-gel method for methylene blue under sunlight

M. Irfan[a*], M. I. Khan[b], M. Al Huwayz[c], N. Alwadai[c]
aDepartment of Physics, University of Okara, 3600, Okara, Pakistan
bDepartment of Physics, The University of Lahore, 53700, Pakistan
cDepartment of Physics, College of Sciences, Princess Nourah bint Abdulrahman University, P.O. Box 84428, Riyadh 11671, Saudi Arabia

Pristine TiO$_2$, Ni-doped, and Cd-doped TiO$_2$ nanocrystals were successfully synthesized by utilizing a single-step sol-gel process. The average particle size (D) of pristine TiO$_2$ was found to be 10.64 nm, while with the addition of Cd and Ni content (0.1) w%, the crystallite size steadily dropped to (10.39 to 8.44) nm. The band gap energies of (0.1) w% Cd and nickel-doped TiO$_2$ are determined (3.20 and 3.07) eV, respectively, which are smaller than that of 3.29 eV for the pristine TiO$_2$. The assessment of the photosensitive activity under visible light irradiation was conducted using the Methylene blue (MB) degradation rate.

1. Introduction

The process of Photocatalysis with semiconductor materials has emerged as a potential and environmentally compatible method for the degradation of organic contaminants in wastewater. According to several recent studies, wastewater discharged from manufacturing industries, including those that produce plastic [1], textile [2][3][4], coatings [5], paints [6][7][8], and inks [9][10], etc. includes a large number of organic pollutants (Dyes) that enter the environment directly. Synthetic dye methylene blue is frequently utilized in a variety of commercial uses and has several harmful effects, i.e. prompting water pollution, harming aquatic environments, direct exposure to MB can cause eye & skin irritation, etc. Despite everything, over the course of wastewater treatment history, numerous studies have examined a variety of treatment techniques. Among these advanced oxidation processes (AOPs) are environmentally friendly, affordable, and effective methods that degrade a variety of contaminant types [11]. Photocatalysis, the technique of using light to catalyze chemical reactions, has shown great promise for the degradation of organic pollutants, air pollution control, and water purification [12][13]. Among various photocatalysts (CdS, TiO$_2$, ZnO, SnO$_2$, WO$_3$) Titanium dioxide (TiO$_2$) has received a lot of attention because of its excellent stability, cost-effectiveness, and non-toxic nature [14][15][16]. The primary drawback of pure TiO$_2$ is that it has a comparatively wide band gap, which restricts its efficiency in using solar light for photocatalytic reactions. Several approaches, such as the addition of metal dopants, have been investigated to improve TiO$_2$'s photocatalytic performance [17][18][19]. Common dopant metals such as Transition metals like (Fe, Co, and Ni), noble metals like (Ag, Au, Cd, and Pt), and non-metals like (N and C) have been used by a variety of material science researchers [20]. When metal dopants are present in TiO$_2$, the band structure is altered due to including new energy levels, which closes the band gap and makes it easier for visible light to be absorbed. In addition, metal dopants can function as co-catalysts by encouraging

---

charge separation lowering the recombination of photogenerated electron-hole pairs, and increasing the overall photocatalytic activity. Dong et.al synthesized Ni-doped TiO_2 nanotubes which show 0.67% photoconversion efficiency, 3.35 times greater compared to undoped TiO_2 nanocrystals[21]. Nakhate et al. prepared Ni-doped TiO_2 catalysts, when exposed to visible light, degraded methylene blue dye 63% more efficiently than that of commercial TiO_2. Karunakaran et al. examined the impact of cadmium (Cd) doping on the photocatalytic activity of TiO_2 and discovered a distinct shift in the optical absorption edge toward the visible region, as well as that Cd doping reduces resistance to charge transfer [22]. Furthermore, Ni element was shown to be the perfect dopant for enhancing the photocatalytic activity of TiO_2, and Ni element doping was shown to increase light absorption by introducing Ni 3d states in the band gap [23][24]. There are several ways of carrying out metal doping, comprising hydrothermal techniques, sol-gel synthesis, co-precipitation, and impregnation process. Numerous benefits come with the Sol-gel method, including low cost, enivroment friedly, suitable reaction time and temperature, and high productivity.

The primary goal of this study is to narrow the bandgap of TiO_2, aiming for a range between 380 and 420 nm. Most materials possess a bandgap in the range of 500 to 600 nm, resulting in the wastage of a significant portion of light. TiO_2, with its inherently high bandgap, offers an opportunity for tuning its Eg within this desired range. The degree of doping significantly impacts the structural/optical properties and efficiency of degradation of TiO_2. Excessive doping can lead to property degradation. Hence, both Ni and Cd have been used as dopants. These elements effectively reduce the recombination rate and enhance the electronic properties of TiO_2, consequently boosting the material's efficiency. This study investigates the influence of Ni and Cd dopants on the optical, morphological, and photocatalytic degradation properties of TiO_2 nanocrystals. Moreover, the photocatalytic degradation of Methylene Blue (MB) dye was conducted under solar irradiation at an intensity ranging between 450 and 500 Wm^{-2}, specifically during peak sunlight hours from 11 am to 3 pm.

2. Experimental

2.1. Materials
All of the precursor ingredients utilized, nickel carbonate, Cadmium Sulphate, and Titanium (IV) butoxide, were acquired from AnalaR and Sigma-Aldrich. The solutions were made with distilled water and a few drops of diluted hydrochloric acid (HCl). No additional purification was performed on any of the components. Different amounts of Ni-doped TiO_2 nanocomposite were prepared by a single-step Sol-gel method.

2.2. Preparation of pristine TiO_2
Precursor 10 ml titanium butoxide (TBO) was added, in 20 ml distilled water, and after 20 min continuous stirring at room temperature (100 K) a few drops of HCl were added dropwise into the solution and steering was stopped after 40 min. For the formation of xerogel abruptly the heated samples were dried in an oven at 150 ^{0}C for 12 hours. The suspension gel shrank during this period as a result of water loss, turning into a thick paste. Bulk crystals subsequently formed, signifying the full drying of the gel. With the help of a mortar and pestle, the dry gel is crushed into fine powder. Calcination at 550 ^{0}C for 4 hr of various concentrations of TiO_2 was followed to remove any suspected contamination that breakdown at high temperatures from the sample

2.3. Preparation of nickle and cadmium doped TiO_2
Precursor 10 ml titanium butoxide (TBO) was added into (0.1g) of $NiCO_3$, and after 20 min continuous stirring at room temperature (27 ^{0}C) 20 ml distilled water and a few drops of HCl were added dropwise into the solution and steering was stopped after 40 min. For the formation of xerogel abruptly the heated samples were dried in an oven at 150 ^{0}C for 12 hours. The suspension gel shrank during this period as a result of water loss, turning into a thick paste. Bulk crystals subsequently formed, signifying the full drying of the gel. With the help of a mortar and pestle, the dry gel is crushed into fine powder. Calcination at 550 ^{0}C for 4 hr of various concentrations of Ni-

doped TiO$_2$ was followed to remove any suspected contamination that broke down at high temperatures from the sample. Similarly above procedure was adapted to prepare a Cd-doped TiO$_2$ sample by adding (0.1g) of Cadmium Suplhate in 10 ml titanium butoxide (TBO).
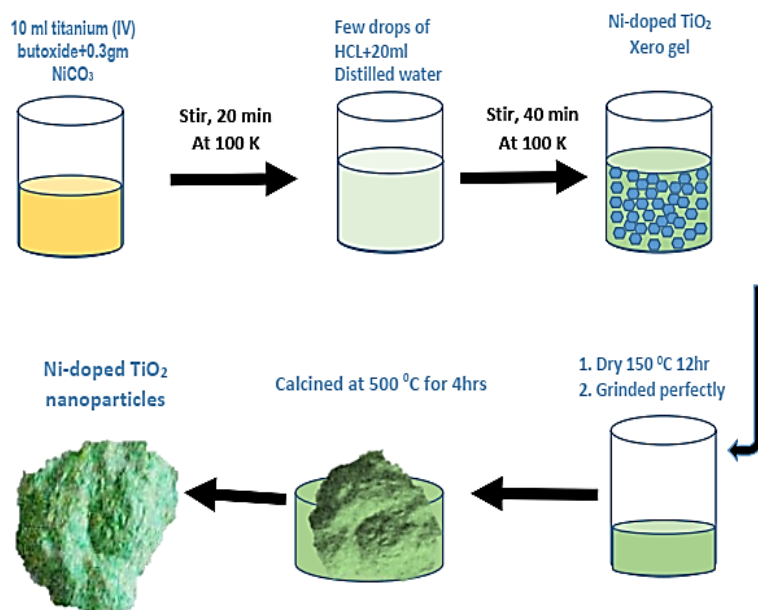

Fig. 1. Schematic illustration of the sol-gel synthesis of pristine TiO$_2$, Ni-doped and Cd-doped TiO$_2$.

2.4. Photodegradation Activity of Pristine, Cd-doped and Ni-doped TiO$_2$

The produced nanocrystals are placed in exposed to the sun, and the rate of photodegradation using methylene blue (MB) at initial dye concentrations of 5 mg per 500 ml is measured for 1 mg of catalysts per 100 ml of dye solution. The samples' UV-vis absorption spectrum was examined by subjecting them to varying durations of visible light exposure in order to determine their photocatalytic potential. With a 15-minute pause, the permitted light exposure duration ranged from 0 to 120 minutes.

3. Results and discussion

3.1. Characterization of Synthesized Pristine and doped TiO$_2$
3.1.1. XRD

Figure 2 depicts the X-ray diffraction patterns (XRD) arrangement of the prepared pure TiO$_2$ and (0.1) w% Ni-doped & Cd-doped TiO$_2$, with the JCPDS card no. 021-1272 (anatase TiO$_2$) and Rutile phase (JCPDS card No 021-1276) respectively. All of the fabricated nanoparticles' XRD patterns showed highly crystalline Anatase peaks at 25.3^0, 38.0^0, 41.5^0, 48.3^0, 55.0^0, and 63.0^0 which correspond to the reflection planes of (101), (210), (211), (220), (300), and (311), respectively, along with peaks at 27.5^0, 36.2^0, and 56.8^0, having reflections planes (111), (200), and (310), adheres to the rutile phase of TiO$_2$ [25][26][27]. Given that there is no significant distinction in the (101), (220), (300), (310), and (311) peak positions of all the synthesized samples, It suggests that as the nickel Cd and Ni is incorporated into the titanium dioxide TiO$_2$ matrix, the material's crystal structure stays mostly unaltered and does not affect the Anatase and Rutile phases in pure and doped samples. Although the peaks (200) and (211) in the Ni-doped TiO$_2$ sample shifted towards higher 2theta degrees. It further reveals that the particles of Cd and Ni were effectively incorporated into the TiO$_2$ lattice because Ni^{+2} ions (0.69 A^0) and Ti^{+4} ions (0.68 A^0) had comparable sizes of their ionic radii, As a result, Ni^{+2} ions substitute Ti^{+4} ions into the TiO$_2$ lattice [28]. In the meantime, the small amount of Ni dopant may be the reason for the

absence of additional Cd and Ni crystallite peaks in the XRD of the generated Ni-doped TiO_2. The average particle size was calculated by using Debye-Scherer's formula presented in equation (1).

$$D = (0.9)\lambda / \beta\cos\theta \tag{1}$$

where θ is the diffraction angle, D is the average particle size, and β is the full-width half maximum (FWHM) of the diffracted peak. Utilizing equation (1), The calculated average size of the crystallite (D) of pristine TiO_2 and (0.1) wt% Cd-doped and Ni-doped TiO_2 nanomaterials were (10.64, 10.39, and 8.44) nm, respectively, shown below in Table 1 and also drawn in Figure (3-b). A decreasing behavior between the dopant concentration and crystallite size was observed [25]. Furthermore, a decrease in the crystallite size resulted due to the substituted ingredients of Cd^{+2} ions and Ni^{+2} ions into the Ti^{+4} lattice and caused significant variations in the intensities of the crystalline peaks shown in Figure 2. This results in an alteration in the percentage crystallinity level (49.5%, 22.4%, and 63.3%) for pure TiO_2, Cd-doped TiO_2, and Ni-doped TiO_2 respectively.
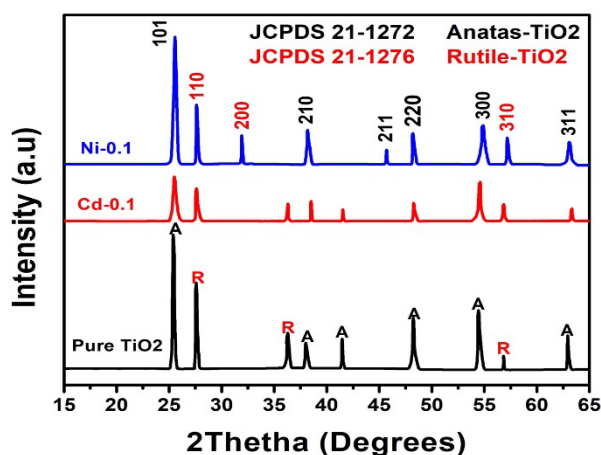

Fig. 2. XRD pattern of pure TiO_2 and Ni-doped & Cd-doped TiO_2.

The dislocation density (dislocations per unit volume) of the fabricated nanocrystals was determined using the relation $(1/D^2)$, where D represents the average crystallite size. The dislocation density is an important parameter that influences both the electrical and mechanical characteristics of nanocrystals. The higher the dislocation density the harder the material. The fluctuation in dislocation density of pure TiO_2 and (0.1) w% concentrations of Ni-doped and Cd-doped TiO_2 is demonstrated in Figure (3-a), and Table 1. The trend of dislocation density increased by adding Cd and Ni concentrations into the TiO_2 lattice, specially drastic increase was observed for the Ni-doped TiO_2 sample 15 times more than that of Cd-doped TiO_2 nanocrystals. Additionally, the crystallinity percentage of Ni-doped TiO_2 increased from 49.5% for Pure TiO_2 to 63.3%, whereas the crystallinity percentage of Cd-doped TiO_2 significantly decreased to 22.4%. A decrease in crystallinity may result from the substitution of Cd ions into TiO_2 crystal lattice because Cd^{+2} ions (148 pm) [29] differ from Ti^{+4} ions (68 pm) in size and electronic structure, which can cause defects and disturb the regular crystalline structure. During the synthesis process, the addition of nickel atoms (69 pm) much smaller in size may influence the nucleation and growth of TiO_2 crystals, leading to a more ordered and structured material[30]. The dislocation density surged as a result of the Ni and Cd ions being incorporated into the TiO_2 crystal lattice, as was previously mentioned in the above paragraph. As a result of these structural imperfections, the crystal structure of TiO_2 may experience microstrain. Ni-doped TiO_2 sample showed a greater strain as compared to Cd-doped TiO_2 as depicted in Figure (3-c).
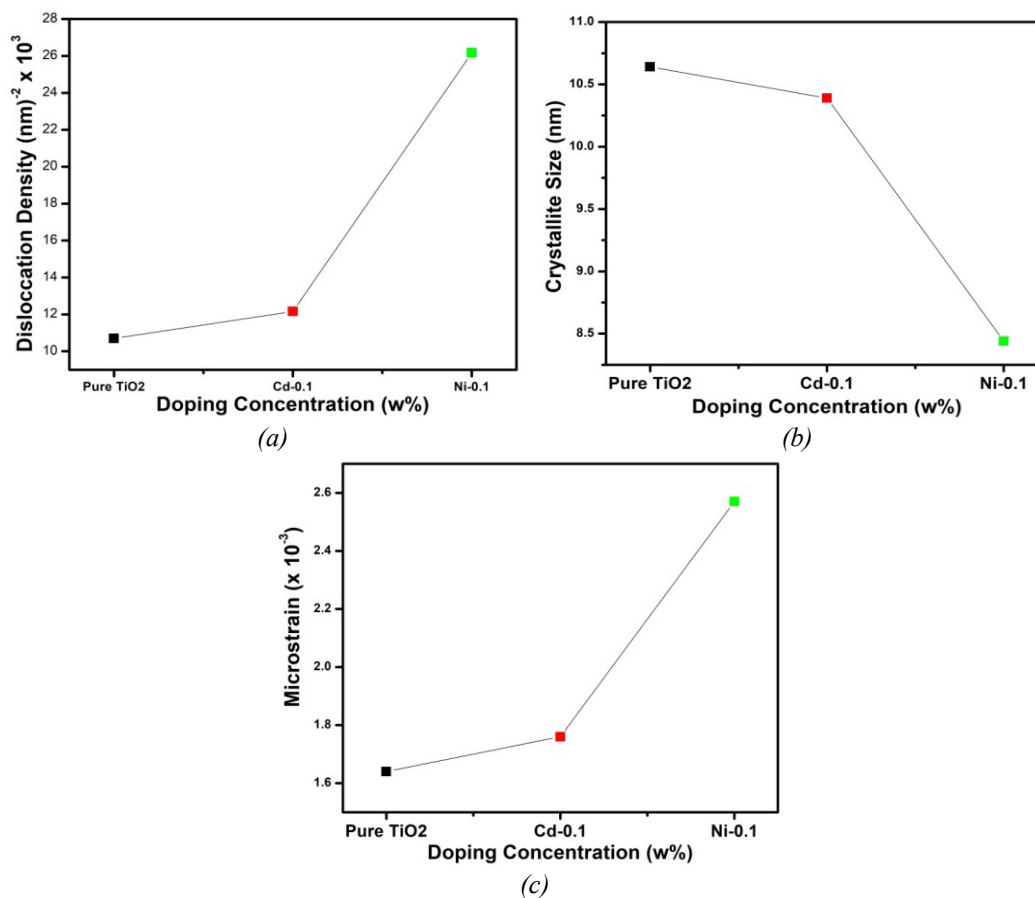
(a) (b)

(c)

Fig. 3. (a) Doping concentration vs Dislocation density (b) Doping concentration vsCrystallite size (c) Doping concentration vs Crystallite size of pristine TiO2, Ni-doped, and Cd-doped TiO2.

Table. 1 Detailed physicochemical properties of pure and Cd & Ni-doped TiO2 nanocrystals.

Dopant Concentration Eg (eV) w%	Crystallite sizes (nm)	Micro strain (10^{-3})	Dislocation Density (nm)$^{-2}$ x 10^3	Crystallinity (%)
TiO_2- pristine 3.29	10.64	1.64	10.69	49.5
TiO_2–Cd 0.1 w% 3.20	10.39	1.76	12.16	22.4
TiO_2–Ni 0.1 w% 3.07	08.44	2.57	26.17	63.3

3.1.2. FTIR Spectra of Ni@TiO₂

Fourier-transform infrared spectroscopy (FTIR) is a useful technique for studying molecule vibrational modes. FTIR spectra of the pure TiO_2 and Cd-doped, Ni-doped TiO_2 samples in the range of 400 Cm^{-1} to 4000 Cm^{-1} are shown in Figure 4. The bending vibration of the metal oxide (Ti-O) bond has been attributed to a peak at around 400 cm^{-1}; Furthermore, the shift in the Cd-O and Ni-O bands towards lower wavenumbers could be attributed to a decrease in particle size [31][32]. The stretching vibrations of the hydroxyl group (OH) or water molecules adsorbed on the material's surface correspond to a peak of around 1500 cm^{-1} [33]. A peak near 1700 cm-1 corresponds to the stretching vibration of the carbonyl group (C=O) in organic materials [34]. This might suggest the existence of organic species or carbon-containing compounds in Ni-doped and

Cd-doped TiO_2 samples. The peak at around 2300 cm^{-1} in titanium dioxide (TiO_2), as well as in Cd and Ni-doped TiO_2, corresponds with the stretching vibration of the triple bond in carbon monoxide (CO) [35]. A significant intensity peak around 3700 cm^{-1} might show the existence of hydroxyl groups (O-H) of Cd-doped and Ni-doped TiO_2 [36]. The appearance of a peak at 3852 cm^{-1} is commonly attributed to the stretching vibration of hydroxyl groups adsorbed on the surface of the material [13][37].
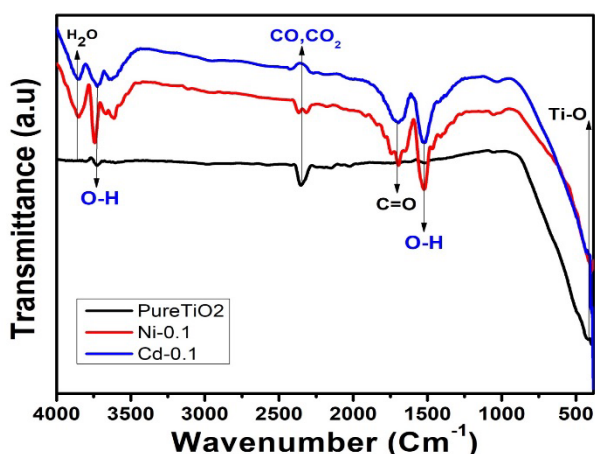
Fig. 4. FTIR spectra of Pure TiO_2, Cd-doped, and Ni-doped TiO_2 nanocrystals.

3.1.3. Raman analysis

Raman spectra of the pure TiO_2 and Cd-dope TiO_2 synthesized samples are shown in Figure 5. Four distinct Raman active modes of pure TiO_2 anatase phase with symmetries Eg, A1g, B1g, and Eg have been noticed at 144, 397, 519, and 639 cm^{-1}, correspondingly [38][39]. The pristine state of anatase TiO_2 was verified by these distinct vibrational frequencies and their corresponding intensity ratios. Both spectroscopies XRD and Raman analyses verify that the anatase TiO_2 phase has formed. Because of cadmium doping into the TiO_2 lattice, the A1g and Eg peaks in the Cd-doped TiO_2 sample show notable shifts with a significant decrease in the peak intensities. Which results in the alteration of the vibrational as well as the electronic properties of the TiO_2.
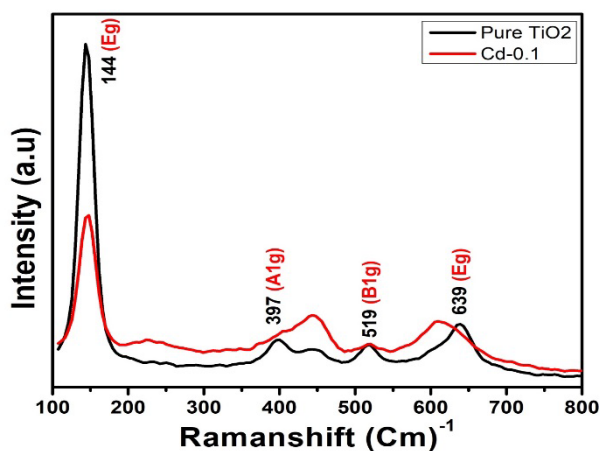

Fig. 5. Raman spectra of pure and cadmium-doped TiO_2.

3.1.4. UV

UV visible spectra and direct band gap of pristine TiO_2, Ni-doped, and Cd-doped TiO_2 synthesized nanocrystals are illustrated in Figure 6. The optically absorbed peaks for pristine TiO_2, Cd-doped, and Ni-doped TiO_2 are observed in the absorption spectrum at (376, 387, and 403) nm respectively. When exposed to UV light, TiO_2 has a band gap of 3.29 eV, which encourages the growth of pairs of electrons and holes. Figure (6-a) shows the absorption spectra of pristine TiO_2, Ni-doped TiO_2, and Cd-doped TiO_2 nanocrystals. A redshift (low energy spectrum) has been shown by doping of Ni ions into TiO_2 crystal lattice. Using the UV absorption data the optical direct band gap of the synthesized materials is determined by using equation (2),

$$(\alpha h\upsilon)^{\gamma} = A(h\upsilon - E_g) \tag{2}$$

where α is the absorption coefficient can be calculated by using a relation $\alpha = \frac{2.302\,A}{t}$, here, t represents the thickness of the thin film (usually 1cm) and A is the absorbance of the material, for indirect allowed transitions $\gamma = 2$. The obtained Indirect band gap values with the help of the Tauc plot, decreased from 3.29 eV for pristine TiO_2 to (3.20 and 3.07) eV for Cd-doped and Ni-doped TiO_2 samples respectively as illustrated in Figure (6-b), it results due to the incorporation of Ni^{+2} and Cd^{+2} ions into the TiO_2 lattice might add extra energy levels into the TiO_2 crystal lattice [40]. These energy levels correspond to the dopant atoms' electrons, where the Ni atoms can occupy the Ti sites. Regarding the initial band gap, electrons can now be excited to these energy levels with less energy.
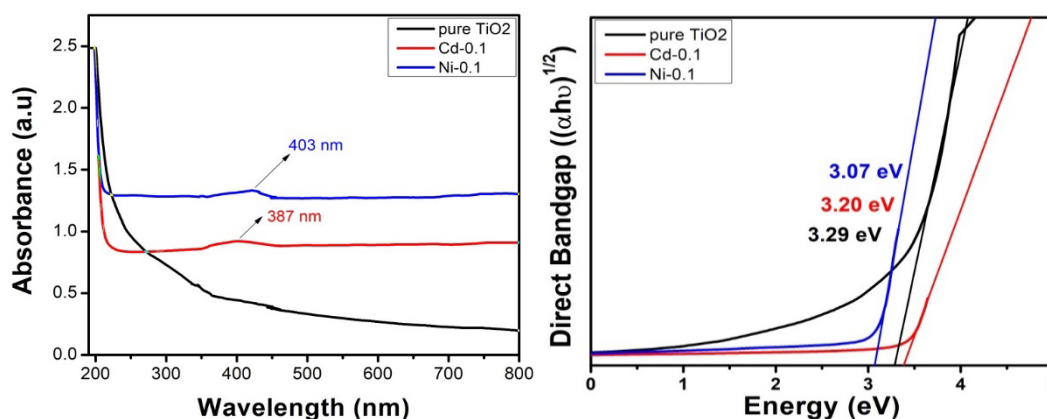

Fig. 6. (a) Absorbance spectra (b) Direct bandgap vs energy, of pristine TiO_2, Ni-doped, and Cd-doped TiO_2 nanocrystals.

Figure (7-a) shows the skin depth, δ, is a measurement that describes the depth in a material at which the intensity of the electromagnetic field drops to roughly 37% of its initial value. The skin depth is determined by using a relation

$$\delta = 1/\alpha \tag{3}$$

where α is the absorption coefficient calculated from UV data. The incorporation of Ni and Cd atoms into the TiO_2 lattice increased the skin depth of the material. In comparison to Ni-doped TiO_2 and pristine TiO_2 nanocrystals, Cd-doped TiO_2 nanocrystals displayed a deeper skin depth of the synthesized material, as seen in Figure (7-a). The addition of dopant materials might enable the Cd and Ni-doped TiO_2 nanocrystals to generate more electron-hole pairs, which may result in increased electrical conductivity and a deeper skin depth of the synthesized materials. These results were also satisfied by the higher dielectric constant of the synthesized materials as depicted in Figure (7-b). higher dielectric constant imaginary part can contribute to the polarizability of the

material, the doping of Cd and Ni shows higher dielectric constant values as compared to pristine TiO_2, hence the polarization mechanism of TiO_2 can be greatly affected by the doping of Cd and Ni.
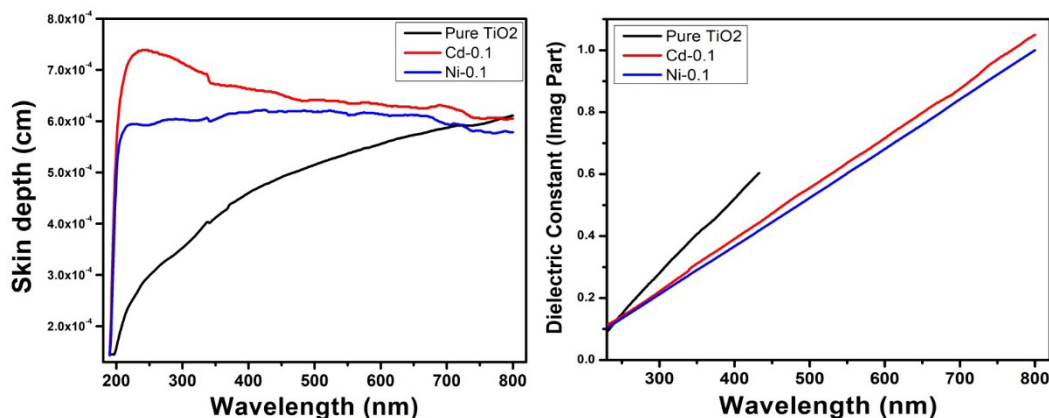

Fig. 7. (a) Skin depth vs. wavelength (b) Dielectric Constant (Imaginary part) vs. wavelength, of pristine TiO_2, Ni-doped, and Cd-doped TiO_2 nanocrystals.

Optical transmittance of the pristine TiO_2, Cd-doped, and Ni-doped TiO_2 nanocrystals is shown in Figure (8-a). Cd-doped and Ni-doped TiO_2 have shown higher transmittance values in the range of 200 nm to 650 nm as compared to pristine TiO_2. The doped nanocrystals show higher transmittance due to the incorporation of Cd^{+2} and Ni^{+2} ions into the TiO_2 lattice due to a decrease in the particle size also mentioned above in the XRD analysis. Optical transmittance of the undoped and doped TiO_2 nanocrystals is calculated by using the equation given below,

$$T = \frac{2n}{n^2+1} \qquad (4)$$

Figure (8-b) represents another valuable optical property of a metal oxide semiconductor the term "extinction coefficient" usually describes a measurement of a material's strength of light absorption at a specific wavelength. The extinction coefficient (k) of a material directly varies with the refractive index as well as the dielectric constant of the material. In this study "k" is determined for pristine and Cd ad Ni-doped TiO_2 by using the following equation,

$$k = \frac{\alpha\lambda}{4\pi} \qquad (5)$$

where α, is the absorption coefficient and λ is the wavelength of incident light. The small values of k in the lower UV region confirm that TiO_2 is a transparent material, although the values of k showed a regular increase for higher wavelengths for Cd-doped and Ni-doped TiO_2 nanocrystals [41].
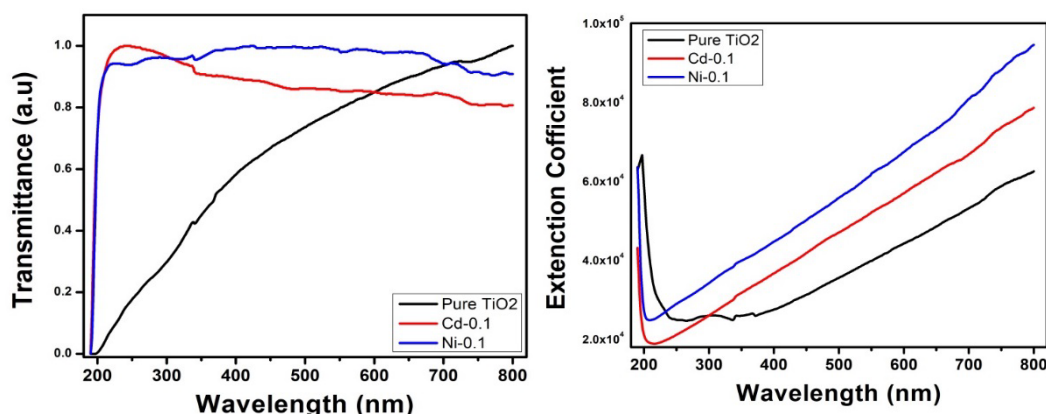
Fig. 8. (a) Transmittance spectra (b) Extinction Coefficient, of pristine TiO₂, Ni-doped, and Cd-doped TiO₂ nanocrystals.

4. Photodegradation activity of MB

The synthesized nanocrystals are exposed to outdoor sunshine, and the rate of photodegradation utilizing methylene blue (MB) 5 mg per 500 ml initial dye concentrations is observed for 1 mg catalysts for each 100 ml of dye solution. The UV-vis absorption spectrum of the samples was analyzed using exposures to visible light for different durations to figure out their photocatalytic capabilities. The assigned light exposure time frame was varied from 0 min to 120 minutes, with a 15-minute delay. For each specific time interval of 15 min MB solution's absorbance is measured at its maximum absorption at a higher wavelength of 465 nm. The electrons in the Ni- and Cd-doped TiO₂ materials were able to move from the valence band to the conduction band due to the energy delivered by sunlight as a level of intermediate excitation of electrons. Redox grounds are created when photogenerated holes and electrons migrate to the surface of nanocrystals (NCs) [42]. These NCs respond with reactants that have been adsorbed, forming hydrogen peroxide, superoxide radical anions, and hydroxyl (–OH) radicals, which are all involved in the oxidation of dye. A steady increase in the degradation efficiency was observed for each synthesized sample with an increase in the duration of time up to 120 min exposure to direct sunlight depicted in Figure (9-a,b,c) for pure, Ni-doped, and Cd-doped TiO₂ nanocrystals. A successive degradation in the MB due to Ni-doped TiO₂ is shown in Figure (9-a), which degrades 23 % of MB in 120 min under the irradiation of sunlight. Figure (9-b) illustrates a significant boost in MB degradation for Cd-doped TiO₂ nanocrystals, with a 33% degradation over the same time duration (120 min). The remarkable photocatalytic efficiency of the Cd-doped and Ni-doped TiO₂ nanocrystals, due to the band gap shifted toward the visible spectrum. The Ni & Cd doping into the TiO₂ lattice might increase the period of existence of the charge carriers which prevents electron/hole recombination for a longer time. Ni/Cd-doped TiO₂ creates new energy levels that raise photocatalytic activity compared to pure TiO₂ and leads to a reduction in bandgap. Although the valency of Cd^{2+} and Ni^{2+} ions is lower than that of Ti^{4+}, consequently, Cd and Ni doping creates oxygen vacancies, which serve as the active sites for water splitting on the metal-doped TiO₂ interfaces. The aforementioned reactive species contribute significantly to the decolorization of MB [43]. Figure (9-d) illustrates the pristine TO₂, Ni, and Cd doped TiO₂ reaction kinetics, which are examined to comprehend the photocatalytic degradation pattern of MB dye using the first-order model. The degradation efficiency of the synthesized samples was determined by using equation (6),

$$\% \text{ Degradation efficiency} = \frac{c_0 - c_t}{c_0} \times 100 \text{ \%} \tag{6}$$

where C_0 and C_t represent the maximum absorption at 465 nm for each synthesized sample at time intervals of 0 min and 15 min delay up to 120 min (t) observing under visible direct sunlight.

Figure (9-d) illustrates how the degradation efficiency of all the synthesized samples increases steadily as the duration of time exposed to sunlight increases. The degradation efficiency of all the synthesized samples increased steadily (15.2%, 23.2%, and 33.1% for pure TiO_2, Ni-doped, and Cd-doped TiO_2 nanocrystals) respectively, when exposed to direct solar radiation.
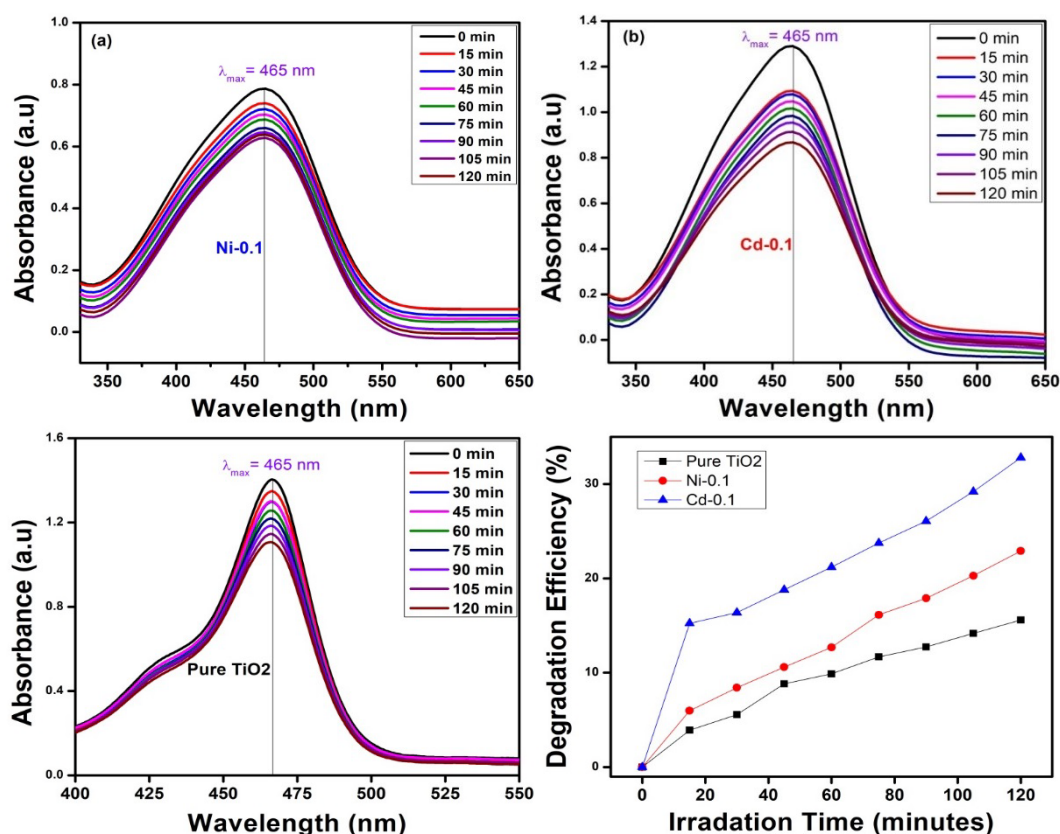

Fig. 9. UV visible spectra of (a) Ni-doped TiO₂ (b) Cd-doped TiO₂ (c) pristine TiO₂, (d) Degradation Efficiency Vs iradtion time of all the synthesized nanocrystals.

Figure (10a,b) shows the first-order model reaction kinetics of pristine TiO_2, Ni-doped, and Cd-doped TiO_2 to comprehend the photocatalytic degradation behavior of MB dye. The following equation (7) given below is used to describe the first-order model kinetics,

$$lnC_0 / C_t = kt \tag{7}$$

where C_0 and C_t represent the amount of MB absorbed at 0-minute and 15-minute intervals up to 120 minutes under direct sunlight. The reaction's time and rate constant are represented by the symbols t and k. Tauc plot was used to evaluate the linear fitting versus irradiation time of the photocatalytic degradation of MB as shown in Figure (10-b). The gradient of the fitting curve yields the value of the assumed kinetic degradation rate constant (k). It was found that the calculated values of (k) for pristine TiO_2, Ni-doped, and Cd-doped TiO_2 are, (0.0014. 0.0020, and 0.0027) min^{-1} respectively under the direct irradiation of sunlight. The Cd-doped TiO_2 sample shows the quickest MB degradation rate and highest kinetic rate degradation rate constant (k=0.0027 min^{-1}) due to abundant charge carriers available for a successful photo-oxidation process.
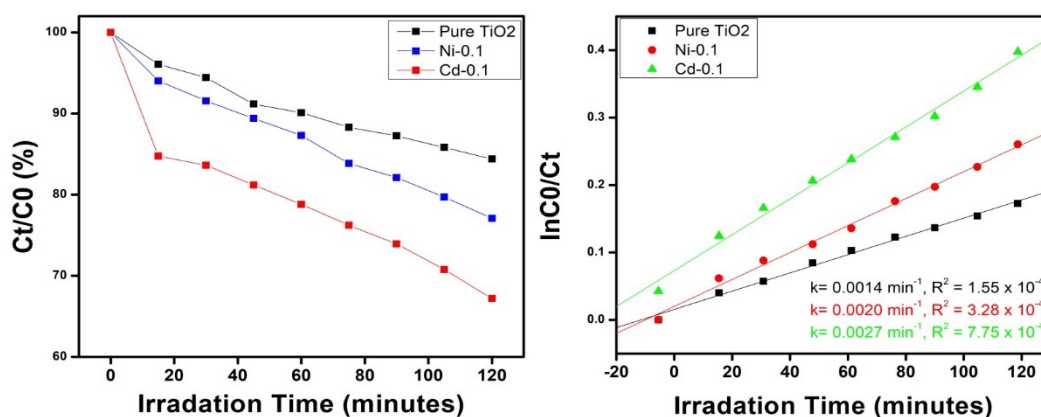
Fig. 10. (a) C_t / C_0 % (b) ln C_0 / C_t Vs Time, of pristine TiO_2, Ni-doped, and Cd-doped TiO_2 nanocrystals.

5. Conclusion

In our study we have successfully synthesized and characterized pristine TiO_2, Cadmium-doped, and nickel-doped TiO_2 nanocrystals, demonstrating their improved photocatalytic performance over pristine TiO_2. Because of the presence of Ni and Cd dopants, which can alter TiO_2's band gap energy and electronic structure, the resultant material has special characteristics. Through XRD analysis, the anatase and rutile phases of the fabricated nanocrystals were verified. When Cd and Ni content (0.1) w% were added, the average particle size of the pure TiO_2 nanocrystal steadily dropped from 10.64 nm to (10.39 to 8.44) nm respectively. Raman spectroscopy also confirmed the anatase phase of TiO_2. UV spectroscopy verified the corresponding optical band gap to be determined are (3.20 eV and 3.07 eV) for Cd-doped and Ni-doped TiO_2 samples, respectively, which somewhat are less than the corresponding band gap values for pristine TiO_2 (3.22eV).

Additionally also analyzed the other notable optical characteristics, such as optical transmittance, absorbance, dielectric constant, and extinction coefficient of the synthesized nanocrystals. From the photocatalytic testing, the Cd-doped TiO_2 nanoparticles showed a greater degradation efficiency for MB of about 33.1 % after 120 minutes of continuous irradiation to direct sunlight. Furthermore, the mechanism and reaction kinetics of photocatalytic MB degradation were examined and schematically displayed. Where Cd-doped TiO_2 samples have the highest kinetic degradation rate constant (k) value (0.0027) min^{-1} among all the synthesized samples.

This research presents an effective strategy that makes it possible to create a new class of metal-doped TiO_2-based reusable nano-photocatalysts that are both efficient and inexpensive and that can be used to effectively degrade MB dye from wastewater treatment, air purification, and renewable energy generation. However, further research is required to optimize the doping concentration and understand the underlying mechanisms governing the improved photocatalytic behavior.

Funding

Author contribution

Acknowledgements

References

[1] B. Suyamud, P. Thiravetyan, G. M. Gadd, B. Panyapinyopol, D. Inthorn, Int. J. Phytoremediation, vol. 22, no. 2, pp. 167-175, Jan. 2020; https://doi.org/10.1080/15226514.2019.1652563

[2] J. Dasgupta, J. Sikder, S. Chakraborty, S. Curcio, E. Drioli, J. Environ. Manage., vol. 147, pp. 55-72, Jan. 2015; https://doi.org/10.1016/j.jenvman.2014.08.008

[3] S. Madhav, A. Ahamad, P. Singh, P. K. Mishra, Environ. Qual. Manag., vol. 27, no. 3, pp. 31-41, Mar. 2018; https://doi.org/10.1002/tqem.21538

[4] G. B. Patel, P. Rakholiya, T. Shindhal, S. Varjani, N. M. Tabhani, K. R. Shah, Bioresour. Technol., vol. 341, p. 125673, Dec. 2021; https://doi.org/10.1016/j.biortech.2021.125673

[5] P. Dhatshanamurthi, M. Shanthi, M. Swaminathan, J. Water Process Eng., vol. 16, pp. 28-34, Apr. 2017; https://doi.org/10.1016/j.jwpe.2016.12.002

[6] S. Varjani, P. Rakholiya, T. Shindhal, A. V. Shah, H. H. Ngo, J. Water Process Eng., vol. 39, p. 101734, Feb. 2021; https://doi.org/10.1016/j.jwpe.2020.101734

[7] S. M. Albukhari, M. Ismail, K. Akhtar, E. Y. Danish, Colloids Surfaces A Physicochem. Eng. Asp., vol. 577, pp. 548-561, Sep. 2019; https://doi.org/10.1016/j.colsurfa.2019.05.058

[8] M. Azad, G. Ali Khan, F. Ismail, W. Ahmed, Inorg. Chem. Commun., vol. 145, p. 109987, Nov. 2022; https://doi.org/10.1016/j.inoche.2022.109987

[9] A. Yaqub, Q. Shafiq, A. R. Khan, S. M. Husnain, F. Shahzad, New J. Chem., vol. 45, no. 22, pp. 9721-9742, 2021; https://doi.org/10.1039/D1NJ00772F

[10] M. S. S. Danish, L. L. Estrella-Pajulas, I. M. Alemaida, M. L. Grilli, A. Mikhaylov, T. Senjyu, Metals vol. 12, no. 5, p. 769, Apr. 2022; https://doi.org/10.3390/met12050769

[11] P. Margan, M. Haghighi, J. Sol-Gel Sci. Technol., vol. 81, no. 2, pp. 556-569, Feb. 2017; https://doi.org/10.1007/s10971-016-4217-7

[12] X. Yang D. Wang, ACS Appl. Energy Mater., vol. 1, no. 12, pp. 6657-6693, Dec. 2018; https://doi.org/10.1021/acsaem.8b01345

[13] S. Zhu, D. Wang, Adv. Energy Mater., vol. 7, no. 23, Dec. 2017; https://doi.org/10.1002/aenm.201700841

[14] S. Manchwari, J. Khatter, R. P. Chauhan, Inorg. Chem. Commun., vol. 146, p. 110082, Dec. 2022; https://doi.org/10.1016/j.inoche.2022.110082

[15] R. B. Rajput, S. N. Jamble, R. B. Kale, J. Environ. Manage., vol. 307, p. 114533, Apr. 2022; https://doi.org/10.1016/j.jenvman.2022.114533

[16] M. T. Uddin, M. E. Hoque, M. Chandra Bhoumick, RSC Adv., vol. 10, no. 40, pp. 23554-23565, 2020; https://doi.org/10.1039/D0RA03233F

[17] S. G. Ullattil, S. B. Narendranath, S. C. Pillai, P. Periyat, Chem. Eng. J., vol. 343, pp. 708-736, Jul. 2018; https://doi.org/10.1016/j.cej.2018.01.069

[18] S. Al Jitan, G. Palmisano, C. Garlisi, Catalysts, vol. 10, no. 2, p. 227, Feb. 2020; https://doi.org/10.3390/catal10020227

[19] J. Prakash, J. Cho, Y. K. Mishra, Micro Nano Eng., vol. 14, p. 100100, Apr. 2022; https://doi.org/10.1016/j.mne.2021.100100

[20] X. Cao, T. Wang, L. Jiao, Adv. Fiber Mater., vol. 3, no. 4, pp. 210-228, Aug. 2021; https://doi.org/10.1007/s42765-021-00065-z

[21] Z. Dong, D. Ding, T. Li, C. Ning, Appl. Surf. Sci., vol. 443, pp. 321-328, Jun. 2018; https://doi.org/10.1016/j.apsusc.2018.03.031

[22] C. Karunakaran, A. Vijayabalan, G. Manikandan, P. Gomathisankar, " Catal. Commun., vol. 12, no. 9, pp. 826-829, Apr. 2011; https://doi.org/10.1016/j.catcom.2011.01.017

[23] N. T. Huong et al., MRS Commun., vol. 13, no. 6, pp. 1119-1124, Aug. 2023; https://doi.org/10.1557/s43579-023-00398-3

[24] K. Feng, C. Wang, X. Hu, J. Fan, E. Liu, Int. J. Energy Res., vol. 46, no. 14, pp. 20828-20837, Nov. 2022; https://doi.org/10.1002/er.8130

[25] M. Baruah, S. L. Ezung, S. Sharma, U. Bora Sinha, D. Sinha, Inorg. Chem. Commun., vol. 144, p. 109905, Oct. 2022; https://doi.org/10.1016/j.inoche.2022.109905

[26] E. Kumi-Barimah, R. Penhale-Jones, A. Salimian, H. Upadhyaya, A. Hasnath, G. Jose, Sci. Rep., vol. 10, no. 1, p. 10144, Jun. 2020; https://doi.org/10.1038/s41598-020-67367-x

[27] F. Scarpelli, T. F. Mastropietro, T. Poerio, N. Godbert, Titanium Dioxide - Material for a Sustainable Environment, InTech, 2018; https://doi.org/10.5772/intechopen.74244

[28] M. A. Mannaa, K. F. Qasim, F. T. Alshorifi, S. M. El-Bahy, R. S. Salama, ACS Omega, vol. 6, no. 45, pp. 30386-30400, Nov. 2021; https://doi.org/10.1021/acsomega.1c03693

[29] W. Braun et al., Proc. Natl. Acad. Sci., vol. 89, no. 21, pp. 10124-10128, Nov. 1992; https://doi.org/10.1073/pnas.89.21.10124

[30] T. He et al., J. Power Sources, vol. 441, p. 227195, Nov. 2019; https://doi.org/10.1016/j.jpowsour.2019.227195

[31] A. M. Hameed, M. A. Hameed, Emergent Mater., vol. 6, no. 2, pp. 627-633, Apr. 2023; https://doi.org/10.1007/s42247-022-00436-1

[32] S. Pavalamalar, M. K. K. Poojha, R. Silambarasan, U. S. S. S. Perisetti, K. Anbalagan, J. Inorg. Organomet. Polym. Mater., Dec. 2023; https://doi.org/10.1007/s10904-023-02940-1

[33] M. Kunnamareddy, R. Rajendran, M. Sivagnanam, R. Rajendran, B. Diravidamani, J. Inorg. Organomet. Polym. Mater., vol. 31, no. 6, pp. 2615-2626, Jun. 2021; https://doi.org/10.1007/s10904-021-01914-5

[34] S. Ijaz, M. Sultana, R. Shamim, N. I. Bukhari, Int. J. Pharm., vol. 633, p. 122584, Feb. 2023; https://doi.org/10.1016/j.ijpharm.2023.122584

[35] H. Esfandian, M. Rostamnejad Cherati, M. Khatirian, Inorg. Chem. Commun., vol. 159, p. 111750, Jan. 2024; https://doi.org/10.1016/j.inoche.2023.111750

[36] T. Munawar et al., Phys. B Condens. Matter, vol. 602, p. 412555, Feb. 2021; https://doi.org/10.1016/j.physb.2020.412555

[37] I. Rahayu, W. Darmawan, D. S. Nawawi, E. Prihatini, R. Ismail, G. D. Laksono, Polymers vol. 14, no. 20, p. 4463, Oct. 2022; https://doi.org/10.3390/polym14204463

[38] D. Rajkumar, H. Umamahesvari, P. Nagaraju, J. Mater. Sci. Mater. Electron., vol. 35, no. 1, p. 32, Jan. 2024; https://doi.org/10.1007/s10854-023-11730-x

[39] S. Challagulla, K. Tarafder, R. Ganesan, S. Roy, Sci. Rep., vol. 7, no. 1, p. 8783, Aug. 2017; https://doi.org/10.1038/s41598-017-08599-2

[40] A. Gordeeva et al., J. Solid State Chem., vol. 322, p. 123952, Jun. 2023; https://doi.org/10.1016/j.jssc.2023.123952

[41] S. M. Al-Shomar, Mater. Res. Express, vol. 7, no. 3, p. 036409, Mar. 2020;

966

https://doi.org/10.1088/2053-1591/ab815b

[42] A. Saleem et al., Mater. Res. Express, vol. 6, no. 1, p. 015003, Oct. 2018; https://doi.org/10.1088/2053-1591/aae28e

[43] T. Ali et al., Mater. Res. Express, vol. 4, no. 1, p. 015022, Jan. 2017; https://doi.org/10.1088/2053-1591/aa576d